Dalton Transactions

Accepted Manuscript

ROYAL SOCIETY OF CHEMISTRY

www.rsc.org/dalton

Journal Name

RSCPublishing

ARTICLE

Synthesis and Spectroscopic Properties of Luminescent Tantalum(V)- β-diketonate complexes and their use as optical sensor and in the preparation of nanostructured Ta_2O_5

Cite this: DOI: 10.1039/x0xx00000x

Received 00th January 2012,
Accepted 00th January 2012

DOI: 10.1039/x0xx00000x

www.rsc.org/

Ana P. Ramos[a], Dayane C.O. dos Reis[a], Rafael R. Pereira[a], Luis G. Dias[a], Rogéria R. Gonçalves[a],

This work proposes a simple and inexpensive method to prepare a new series of β -diketonates-tantalum complexes. The method is based on the use of $[TaF_7]^{2-}$ solution, as tantalum precursor, thenoyltrifluoroacetone (TTA), hexafluoroacetylacetone (HFA), and benzoyltrifluoroacetylacetone (BFA) in basic medium; basic pH is achieved by adding urea into the reactional medium. Elemental analysis, H^1-NMR spectroscopy, potentiometric measurements conducted with a fluorine-selective electrode, conductivity measurements, vibrational spectroscopy based on quantum chemistry calculations, and electronic spectroscopy, helped to determine the molecular structure of the complexes. At room temperature in the solid state and in solution upon irradiation with UV light, the complexes exhibited blue emission, probably as a result of the heavy atom effect. On the basis of the structures, luminescence properties at room temperature, and solvent-dependent changes in the electronic properties of the complexes, these β-diketonates are potentially applicable as optical ethanol or humidity sensors and are promising materials for the development of luminescent devices.

1. Introduction

Literature works have reported on inorganic β-diketonate complexes containing first-row of transition metals and lanthanides since the early 1940s[1, 2]. On the other hand, publication on the structural properties of this kind of complexes bearing metals like Ta (V) and Nb (V) are scarce and their synthesis usually involves laborious and expensive synthetic routes[3-5]. In recent works, the preparation of tantalum complexes involves mostly metal alkoxide as precursor for obtaining alkoxide-derived tantalum complexes[6].

The importance of synthesizing Ta(V) and Nb(V) β –diketonate complexes lies mainly on their use as precursors of nano- or microstructured oxides with applications in such diverse fields as microelectronics to fabricate semiconductor components[7], production of various types of reaction catalysts[8, 9], and preparation of materials with special physicochemical characteristics, like planar waveguides[10-12]. In addition, the use of metal complexes as precursors to produce thin films via metal organic chemical vapor deposition (MOCVD) has raised researchers' interest in obtaining these complexes and understanding their properties.

Moreover, β-diketone metallic complexes are attractive materials to fabricate light emitting devices like OLEDS[13]. In particular, some rare-earth β-diketonate complexes are useful as OLEDS: they display characteristic narrow emission bands attributed to 4f-4f electronic transitions in the visible range and relatively longer lifetimes of rare earth excited state, giving rise to interesting photo and electroluminescent materials[13].

In the solid state, most β-diketonate complexes containing transition metals only exhibit phosphorescence at very low temperatures (i.e. 77 K). However, some of these complexes present phosphorescence at room temperature, which enables their application in photonics, including light-emitting diodes[14, 15], and photovoltaic devices[16]. These complexes have also attracted the attention of scientists working in the field of optical sensors[17, 18] – they display considerable Stokes displacement, which facilitates separation of excitation and emission, not to mention that the latter phenomena have

relatively longer lifetimes as compared with organic luminophores.

With the aid of luminescence at low temperature and Raman studies, Wexler et al.[19] assigned the emission band present in the spectra of these β-diketonate complexes to the ligand-centered π-π* electronic transition. Therefore, the radiative process typically originates from the lowest energy triplet state of the ligand. In the case of the complexes, the presence of the heavy metal decreases the radiative lifetime of triplets due to increased spin–orbit coupling. Nevertheless, at room temperature, the intraligand phosphorescence is hardly detectable[20]. Phosphorescence will only be detectable if the emitting triplets exist at energies below the other possible excited states, such as metal-centered (d-d or f-f intraconfigurational transitions) or charge transfer (CT) states, which can be populated by a nonradiative process from the betadiketonate intraligand excited states. Depending on the energy of the triplets and the other excited states, luminescence or quenching can occur.

Whereas numerous metallic complexes that emit red or green phosphorescence, meet this requirement, finding triplet emitters with a blue luminescence is rather difficult[21], since the common presence of an interfering ligand field (LF) and/or CT states provide luminescence quenching.

Choosing an appropriate ligand with desired triplet energy and a heavy metal that does not participate in low-energy electronic transitions is a very simple strategy to overcome this issue. Strasser et al.[20] prepared hexafluoroacetylacetone (HFA) complexes using s^2 metals like Pb (II), Tl (I), and Bi (III); in the solid state, these complexes displayed phosphorescence under ambient condition, but complexes in solution had no phosphorescence.

Although metals with a closed shell of valence electrons may be less suitable for phosphorescence because the heavy atom effect is only partially transmitted to the ligand or not transmitted at all[20], in the present work we prepared a series of β-diketonate complexes with Ta (V), which exhibit blue luminescence at room temperature in both the solid state and solution. We solved the structures of these complexes and investigated their luminescent properties at room temperature, which pointed to their potential use as optical ethanol or humidity sensors (denoted by the solvent-dependence of electronic properties) and as precursors to prepare nanostructured Ta_2O_5 with structural properties that depend on the β-diketonate complex.

2. Experimental Section

2.1. Materials

A tantalum fluoride aqueous solution (pH 1.0) kindly provided by *Companhia Industrial Fluminense*, Brazil was the starting material to prepare all the complexes. In this solution, the metallic center is coordinated with seven fluorine atoms, to form an ion complex with structure $[TaF_7]^{2-}$ [22, 23]. Thenoyltrifluoroacetone (TTA), hexafluoroacetylacetone (HFA), and benzoyltrifluoroacetone (BFA) (sigma-aldrich 99%) were used as received. β-diketones 1.0 $mol.L^{-1}$ were prepared and used as starting material in the synthesis.

2.2. Synthesis of the β-diketonate complexes

The Ta(V)-β-diketonates complexes were synthesized by mixing 1.4 mL of the tantalum aqueous solution (0.2 $mol.L^{-1}$) with 560 µL of the β-diketonates ethanolic solution 1.0 $mol.L^{-1}$ (with a 1:2 of Ta(V)/β-diketone molar ratio) in a plastic flask containing 7 mL of urea solution 1.0 $mol.L^{-1}$. The mixtures were kept in a water bath at 80 ºC, for 6 h, to guarantee total decomposition of the base[24]. After 6 h the reaction was stopped with the aid of an ice bath. The resulting solution was dried at 70 ºC in an oven. Then, the obtained solid was washed three times with ethanol with the help of a vacuum filtration system, which removed excess β-diketone and urea. The complexes $[TaTTA(NH_3)_3F_2]F_2$; $[TaHFA(NH_3)_3F_2]F_2$; and $[TaBFA(NH_3)_3F_2]F_2$ were labeled as TaTTA, TaHFA and TaBFA, respectively.

2.3. Synthesis of the nanostructured Ta_2O_5

Thermal annealing of the complexes were carried out at 900 °C, 1000 °C and 1100 °C for 4 h, which afforded nanocrystalline tantalum oxide.

2.4. Methods

The initial structure of the complex was prepared with VegaZZ[25-27]. Then, the geometry was fully optimized at the PBE1PBE[28] level using the 6-31G* Pople basis set[29] for all the atoms other than Ta. For optimization of Ta element, the LANL08 basis set[30] with effective core potential was employed. Tight conditions were also used for self-consistent field and geometry convergence. Theoretical infrared spectra were generated by the unscaled harmonic frequencies (only real numbers were found). Oscillator strengths were calculated on the complex with fully optimized geometry at the PBE1PBE level and basis set cited above. All the DFT calculations were performed with the aid of the program Gaussian 03, revision B.04[31].

Fourier transformed infrared (FTIR) spectra of the complexes in solid state were recorded on a Bomem-MB 102 spectrometer, in KBr pellets. The UV-Vis absorption spectra of the complexes dissolved in water and ethanol were registered on a Vectra XM Hewlett Packard HP 8453 spectrometer; a quartz cell with optical path of 1.0 cm was employed. The emission spectra in the visible range were collected on a SpexTriax 550 Fluorolog III spectrofluorometer. The samples were also analyzed by H^1-NMR (Brüker AVANCE 500 operating at 500.13 MHz) and carbon and hydrogen elemental analysis at room temperature. For the H^1-NMR analysis of the β-diketones and the β-diketonate complexes, deuterated chloroform ($CDCl_3$), and deuterated water (D_2O) or deuterated ethanol (C_2D_5OD) were used as solvent respectively, and tetramethylsilane (TMS) as the internal reference. Conductivity measurements were carried out on a Metrohm 712 conductivimeter to determine the number of ions present in solution[32, 33] as well as the charge of the

complex ion, and the concentration of fluoride ions present as counterions. The latter determination relied on a fluoride selective electrode. The concentration of the complexes in the aqueous solutions used during the conductivity studies was 1.0 mmol.L^{-1}, further dilutions were also used. A sodium fluoride aqueous solution (pH 5.5 TSAB buffer) was used as standard to construct a standard curve potential (mV) vs fluoride concentration. All the measurements were accomplished at room temperature. The molecular mass of the TaTTA complex was determined using a MALDI ultrafex TOF/TOF 4AP17 Bruker (voltage polarity POS and number of shots 600), in the Reflector acquisition operation mode.

The product of the decomposition of the complexes after thermal treatment were characterized by X-ray diffractometry (XRD), which was performed on a Siemens–Bruker D5005-AXS diffractometer, with Cu Kα radiation, graphite monochromator, k = 1.5418 Å, in the 10–80° 2θ range. The scanning electron microscopy (SEM) images were acquired on an Electronic Scanning Microscope Zeiss EVO50, coupled to an Energy Dispersive Spectrophotometer (EDS)500 digital processing IXRS Systems Inc.

3. Results

3.1. Structure of the Tantalum(V)- β-diketonate complexes

All the complexes were highly soluble in ethanol and water, but they were not soluble in organic solvents like chloroform and acetylacetone (acac). The conductivity data helped to determine the number of ions present in solution related with the charge of the complex ion and its counterions. The molar conductivity of the complexes (see Table 1) showed that three ions existed in solution[32]: a cation with charge 2+ and two fluoride ions as counterions. On the basis of the elemental analysis and mass spectrometry data (to will be discussed below), the only structure that would result in charge 2+ for the β-diketonate complex has two Fluor atoms and one β-diketone molecule coordinated to the metallic center (Figure 1). Conductivity measurements with the aid of a fluoride selective electrode helped to determine the concentration of fluoride ions as counterions in the aqueous solution of the complex. The experimental values agreed with calculated values when we considered that each mol of the complex contained 2 mols of F^- (Table 1). The concentration of the aqueous solutions of the complexes employed to measure the fluoride-selective electrode potential (E) and to calculate the theoretical concentrations of F^- were: TaTTA 8.4 x 10^{-4} mol.L$^-$; TaBFA 1.0 x 10^{-3} mol.L^{-1}; and TaHFA 9.4 x 10^{-4} mol.L^{-1}.

Table 1: Molar conductivity and fluoride concentration in aqueous solution for the coordination compounds.

Samples	*Molar conductivity ($\Omega^{-1}cm^2$ $mol^{-1}L$)*	*Number of ions*	*E (mV)*	*[F$^-$] calculated (mg/L)*	*[F$^-$] experimental (mg/L)*
TaTTA	293	3	-43.6	31.0	37.2
TaBFA	277	3	-47.0	40.0	43.6
TaHFA	241	3	-41.2	35.6	33.0

The TaTTA complex contained 18.21% C, and 2.98% H. We proposed $[TaTTA(NH_3)_3F_2]F_2$ as the structure of TaTTA, which corresponded to 18.15% C; and 2.65% H (calculated). On the basis of mass spectrometry, the mass of the complex divided by its charge (m/z) was 246.99 g.mol^{-1}. The couterions were not taken into account. The m/z calculated for the complex was 246.11 g.mol^{-1}, which agreed with the experimental data.

The ^{1}H-NMR features and the FTIR spectroscopic data obtained for the TaTTA compound supported the $[TaTTA(NH_3)_3F_2]F_2$ structure. The ^{1}H-NMR spectra displayed resonance peaks in the δ 1.0- 3.9 ppm range (relative to TMS). These peaks referred to amine groups, which appeared as two multiplets due to coupling between the protons present in each NH_3 group. These multiplets were integrated for nine protons; hence, three amine groups coordinated to the metallic center. The spectrum also presented peaks typical of TTA protons, which emerged as a multiplet between δ 7.84 and 8.06 ppm. The triplet at δ 7.22 ppm corresponded to the protons of the thenoyl ring[34]; therefore, the structure of β-diketone was preserved after complexation. The singlet peak at δ 14.5 ppm due to the hydroxyl proton of the ligand did not arise in the spectrum of the complex, which showed that this proton was lost during chelation.

Taking all the results of conductivity measurements, elemental analysis, ^{1}H-NMR spectroscopy and mass spectrometry into account, we proposed $[TaTTA(NH_3)_3F_2]F_2$ as the structure for the complex containing the TTA β-diketone. On the basis of the analogous experimental procedures, conductivity measurements and the concentration of fluoride as counterions, we obtained strong indication that BFA and HFA afforded the complexes $[TaBTA(NH_3)_3F_2]F_2$ and $[TaHFA(NH_3)_3F_2]F_2$. Figure 1 shows the optimized geometry of the $[TaTTA(NH_3)_3F_2]F_2$ complex (please see section 2.4 for details on calculation). Vibrational and electronic structural properties, discussed as follows, corroborated with these structural data.

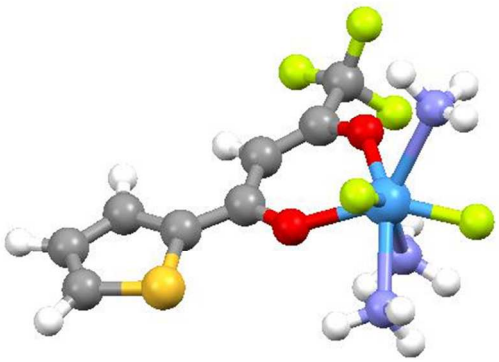

Figure 1. Optimized geometry of the TaTTA complex. The different colors refer to the Oxygen (red), Fluor (green), Nitrogen (purple), Carbon (Gray), Hydrogen (white), Sulfur, (yellow), and Tantalum (blue) atoms. Tantalum (V) is represented as being heptacoordinated.

3.2. Vibrational structure

Figure 2 (I) depicts the FTIR absorption spectra of TTA (Figure 2 (I) (A)) and TaTTA complexes (Figure 2 (I) (B)). Table 2 summaries the positions and the assigments of the bands present in the FTIR spectra of pure TTA and TaTTA. The assignments of pure TTA relied on a previous work published by Uzoukwu[34]. As for the complex, the attributions of the FTIR bands were based on the theoretical infrared spectrum generated as described in section 2.4.

Table 2: Attribution of the bands in the FTIR spectra of the TaTTA complex

Peaks (cm^{-1}) TaTTA complex Experimental	Peaks (cm^{-1}) TaTTA complex Theoretical	Peaks (cm^{-1}) TTA Experimental	Assignments
		3440	νO=H enol[34]
3448	3445		ν_sN-H
3340	3440		ν_{as}N-H
3256	3276		ν_{as}C-H
1682	1694		Twist N-H
		1640	ν_sC=O[35]
1623	1689		bend N-H + deformation of chelate ring
1603	1602		ν_{as}Ta=O + deformation of thenoyl and chelate ring
1597	1514	1575	Deformation of thenoyl and chelate ring[35]
		1407	Thenoyl ring stretch[35]
1470	1460		νTa-NH_3 + ν_sTa=O + deformation of thenoyl ring
1406			νTa-NH_3
		1308	$\nu_{as}CF_3$[35]
1270	1280		$\nu_{as}CF_3$
		1194	β_sC-H[35]
1211			
1155	1148		ν_{as}Ta=O + C-H in plane deformation + C-F bending
		1140	β_sC-H[35]
		1103	ν_sCF_3[35]
		1063	C-H in plane deformation of thenoyl ring[35]
985	978		ν_{as}C-H
		860, 804, 735	C-H out-of-plane deformation of thenoyl ring[35]
743	739		ν_{as}N-H + chelate ring vibration + ν_{as}Ta-F + C-H out-of-plane deformation of thenoyl ring + n_sTa=O
		582	βCF_3[35]
526	514		Scissoring of C-H in thenoyl ring + scissoring of Ta-F + scissoring of C-F
560	546		Thenoyl ring stretching + ν_{as}C-H + n_sC-F
483	458		

The split bands that appeared at about 3450 cm^{-1} were typical of N-H stretching. The band at 1470 cm^{-1} corresponded to the vibrational modes of the Ta-NH_3 bends, which attest that NH_3 groups coordinated to the metal. The band at 743 cm^{-1}, assigned to νTa-F, indicated Ta-F coordination. The prominent IR feature found in the spectrum of pure TTA at 1640 cm^{-1} (Figure 2 (I) (A)) and Table 2) corresponded to carbonylic stretching. For the complex, this band emerged at 1603 cm^{-1} (Figure 2 (I) and Table 2), as a consequence of β-diketone coordination to the metallic center. Comparing the FTIR spectrum of pure BFA (Figure 2 (I) (C)) with the spectrum of the complex TaBFA (Figure 2 (I) (D)), the band attributed to C=O stretching shifted to lower wavenumbers after complexation, attesting that the metal bound to this group. The number of bands in the region between 1400 and 580 cm^{-1} decreased, because the BFA structure became stiffer after complexation. We verified a similar behavior for the FTIR spectra of pure HFA (Figure 2 (II) (A)) and TaHFA (Figure 2 (II) (B)). Some bands like the broad band at ~514 cm^{-1}, attributed to Ta-F and O=Ta=O scissoring, arose in the FTIR spectra of the complexes but were absent from the spectra of the pure β-diketones, which confirmed that the fluorine atoms coordinated to the metallic center. Moreover, the broad band at 3400 cm^{-1} ascribed to the O-H stretching of the enol group, disappeared after complexation. Therefore, the oxygen atoms coordinated to the metallic center were removed. Removal of the enolic proton was evident after comparison of the ^{1}H-NMR spectra of pure TTA and TaTTA.

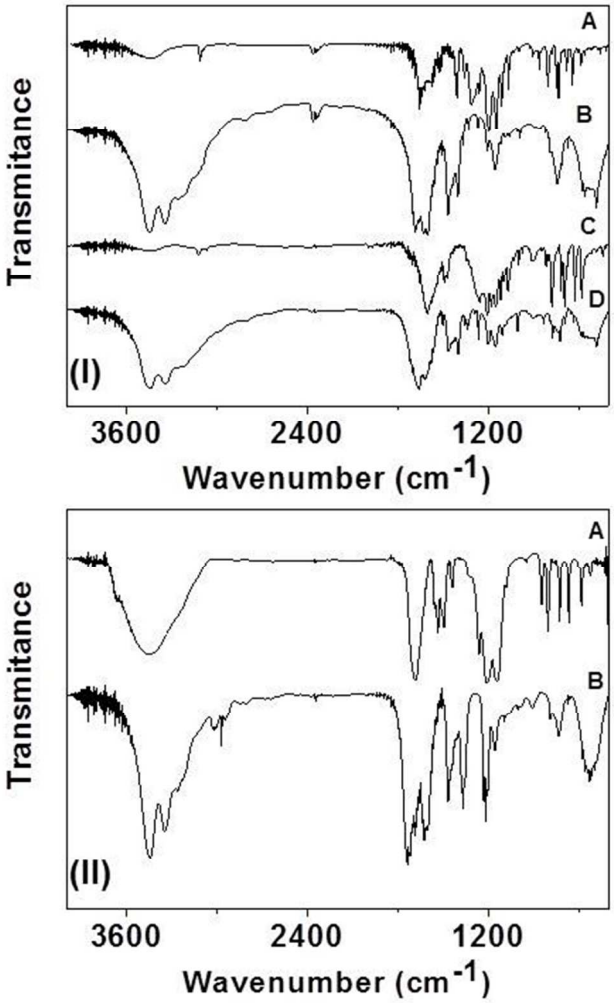

Figure 2. (I) FTIR spectra of (A) pure TTA, (B) and TaTTA , (C) pure BFA, and (D) TaBFA; and (II) FTIR spectra of (A) pure HFA, (B) TaHFA.

3.3. Electronic Properties: Absorption and Luminescence studies

The UV-VIS absorption spectrum of the complexes helped to investigate the effect of the complexation between β-diketone and Ta(V) ions on the electronic properties. Upon complexation with Ta(V), the band corresponding to the spin-allowed π-π* electronic transition of the β-diketone changed[22]. Figure 3 (A) shows the UV-VIS absorption spectra of pure TTA and TaTTA. We normalized the absorption spectra of all the compounds and β-diketones, to observe shifts and other changes better. The band at 292 nm, assigned to the lowest energy spin-allowed π-π* intraligand transition, shifted after complexation, showing that the heavy atom effect reduced the energy of the b-diketone triplet, as shown by Strasser et al.[20] in their study of Pb^{2+}-β-diketonate complexes. This red-shift could also be a consequence of increased system resonance[35]. The band at 265 nm corresponded to the n-π* electronic transitions related to the π-conjugated bonds present in the thenoyl group of TTA[19]. The position of this band did not change after complexation.

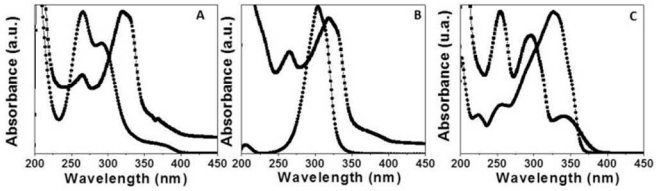

Figure 3: UV-Vis absorption spectra in the UV-Vis region of (•) pure TTA and (■)TaTTA in ethanol (A), (•) pure HFA and (■) TaHFA in ethanol (B), and (•) pure BFA and (■)TaBFA in ethanol (C). The intensities of the spectra are normalized.

Figure 3 (B) brings the UV-VIS absorption spectra of pure HFA and TaHFA. The band at 303 nm (also attributed to the π-π* electronic transition) in the spectrum of pure HFA is also shifted to the red after complexation. The absorption spectrum of BFA, in Figure 3 (C), was more complex. BFA bears a benzoyl ring, which strongly absorbs in the UV-VIS region. The band at 326 nm is shifted to 338 nm after complexation, and its relative intensity diminished. Table 3 lists the position of the absorption bands of pure β-diketones and complexes.

Table 3: Absorption bands of pure b-diketones and complexes

Sample	*Band 1 (nm)*	*Band 2 (nm)*	*Band 3 (nm)*
TTA	265	292	
TaTTA	265	320	
BFA	223	254	326
TaBFA	254	296	338
HFA	205	303	
TaHFA	264	319	

The UV-Vis spectra and the molar absorptivities calculated for the maximum absorption band (Table 4) of all the complexes changed upon dissolution in water or ethanol, Figures 4 (A), (B), and (C). The molar absorptivity coefficients of the pure b-diketones TTA, BFA, and HFA in ethanol were 6482, 13689, and 4813 $L.cm^{-1}.mol^{-1}$, respectively.

Table 4: Molar absorptivity coefficient determined for the b-diketonate complexes in water and ethanol

Sample	*ε (cm^{-1} mol^{-1}.L) in ethanol*	*ε (cm^{-1} mol^{-1}.L) in water*
TaTTA	4431	3320
TaBFA	3073	5204
TaHFA	228.9	143.8

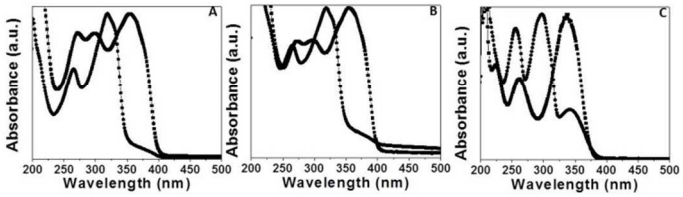

Figure 4: Absorption spectra in the UV-Vis region of (A) TaTTA, (B)TaHFA, and (C) TaBFA in ethanol (•) and in water (■). All the spectra are normalized.

Remarkable changes have been observed in the absorption spectra of the complexes in water and ethanol. The Figure 5 brings absorption features of TaTTA complex dissolved in different solutions, which has varied water/ethanol (v/v) concentration. The absorption spectra were normalized at 320 nm.

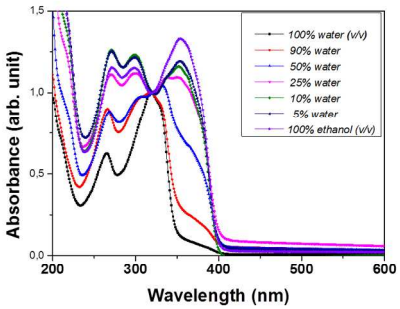

Figure 5: Absorption spectra in the UV-Vis region of TaTTA complex in different volume ratio of water ethanol and water. All the spectra are normalized at 320 nm.

The emission spectrum of TaTTA also changed upon dissolution in water and ethanol (Figure 6). In more polar solvents the bathochromic displacement of the bands related to the π-π* electronic transitions was associated with the smaller difference in the energy between these two states due to stabilization of the excited state. This feature makes the complexes potentially applicable in the field of humidity/ethanol optical sensors.

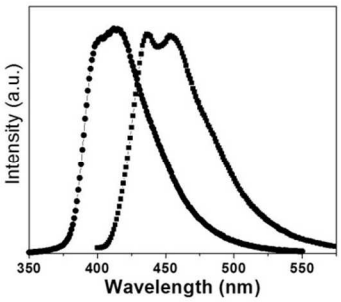

Figure 6: Emission spectra of TaTTA in water (•) and in ethanol (■). $\lambda_{excitation}$= 290 nm.

Figure 7 displays the emission spectra of the pure β-diketones (TTA, BFA, and HFA) in the solid state, as well as the emission spectra of the aqueous solutions containing TaTTA, TaBFA, and TaHFA recorded at 298 K. All the spectra were acquired at a fixed excitation wavelength of 290 nm, and the emission intensities were normalized for better comparison. Whilst in the case of pure β-diketones only the solid samples displayed emission, complexes in solution and in the solid state emitted at room temperature. Dissolution of β-diketones elicited large the multiphonon relaxation and suppressed the radiative emission. Ta atoms exerted the heavy atom effect, so radiative emission occurred for all the complexes. In addition, the luminescence of the complexes in water and ethanol suggested that a more rigid structure emerged in the complexes as compared with the pure β-diketones.

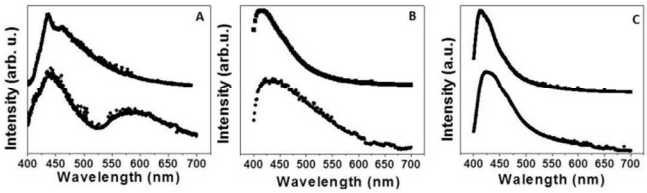

Figure 7: Emission spectra of (A) (•) pure solid TTA and (■) TaTTA in water; (B) (•) pure HFA and (■) TaHFA in water, (C) and of (•) pure BFA and (■) TaBFA in water. $\lambda_{excitation}$ = 290 nm.

We maintained the apertures of the emission and excitation slits of the fluorimeter at different positions, which resulted in a bandwidth of 1 nm and 4 nm when we acquired the spectra of the complexes and of the pure β-diketone, respectively.

Complexation with Ta modified the emission spectra of the β-diketones (Figure 7). In the presence of this metal, the emission maximum of BFA and HFA shifted toward the blue, and the full width at half-maximum (FWHM) of the bands diminished (Figures 7B and 7C). The spectrum of the complex formed between TTA and Ta (Figure 7A) revealed a defined vibronic structure. The broad band at 580 nm in the emission spectrum of pure TTA (Figure 7A) corresponded to interligand charge transfer due to formation of excimer. Upon complexation, this band disappeared, because the approach of the ligand became more difficult[36].

The emission spectra of TaBFA and TaHFA (Figures 7 B and C) presented a single broad band with approximately the same onset energy at about 24000 cm^{-1}. Wexler et al.[19] have shown that the values of onset energy are similar for acac-derived β-diketonates. Small shifts occurred because the substituents (CF_3, thenoyl and benzoyl rings) perturbed the p orbitals. The FWHM of the bands was 2703 cm^{-1} and 5154 cm^{-1} respectively. In contrast, the spectrum of TaTTA (Figure 7A) evidenced resolved vibronic structure with E_{00} of about 22833 cm^{-1} and FWHM of 4086 cm^{-1}. The main progression had spacing of 1420 cm^{-1}. The FTIR spectrum of TaTTA (Figure 2A) displayed a band at about 1450 cm^{-1}, which confirmed the vibronic structure of the complex. This band appears only in the spectrum of the complex and not in the pure TTA spectrum.

3.4. Nanostructured Ta_2O_5

Figure 8 shows the X-ray diffraction pattern of the complexes TaTTA and TaBFA after thermal treatment at 900 °C for 4 h. The annealed TaBFA sample (Figure 7 B) presented several peaks, centered at 2θ = 22.9, 28.4, 36.8, 46.9, 50.1, 50.7, and 55.7, assigned to the exclusive formation of orthorhombic Ta_2O_5[37]. As for TaBFA, there was evidence for a small quantity of other crystalline phases apart from little intense peaks, similar to those found for TaTTA, corresponding to orthorhombic Ta_2O_5 (JCPDS 00-054-0514 and JCPDS 01-070-4775), and in addition we detected a large background between 15° and 40° in 2θ, which corresponds to the amorphous tantalum-based host[38, 39].

Figure 8. Powder X-ray diffraction patterns of the complexes (A) TaTTA, and (B) TaBFA, annealed at 900 °C for 4 h.

Thermal treatment of TaTTA complex (Figure 8A) afforded a mixture of the same orthorhombic Ta_2O_5 crystalline phases observed previously, even for the complex annealed at higher temperatures, but the phase percentages were different. Figure 9 shows the XRD diffractograms of TaTTA annealed at 900 °C, 1000 °C, and 1100 °C. The diffraction patterns revealed at least three different orthorhombic Ta_2O_5 phases. As the temperature augmented, the crystalline phase corresponding to orthorhombic Ta_2O_5- JCPDS 00-054-0514 increased and the halo, corresponding to the amorphous phase, disappeared completely.

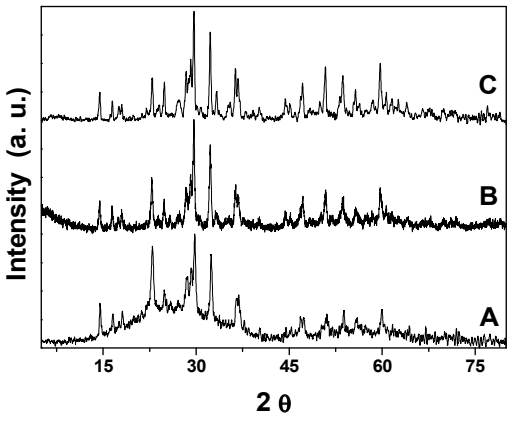

Figure 9. Powder X-ray diffraction patterns of the complexes TaTTA annealed at (A) 900 °C for 4 h, (B) 1000 °C for 4 h, (C) 1100 °C for 4 h.

SEM analysis of TaTTA annealed at 900 °C provided information about morphology and composition. Figure 10 A brings SEM images of the nanoparticles prepared via thermodecomposition of TaTTA and clearly evidences spherical-like nanostructures with grain size smaller than 100 nm. The crystallite size estimated from the XRD analysis in this case was about 11 nm, which indicated that the grain observed by SEM was not a single cystal. It can be observed that the small particles (spherical-like nanoparticles) form both the large formless and needle-like aggregates which can be related to the amorphous and crystalline phases observed by XRD. Figure 10 B also displayed the EDS analysis, which detected only Ta and O atoms and dismissed the presence of products containing fluoride and carbon (at least for concentration higher than 10,000 ppm), corroborating with XRD analysis.

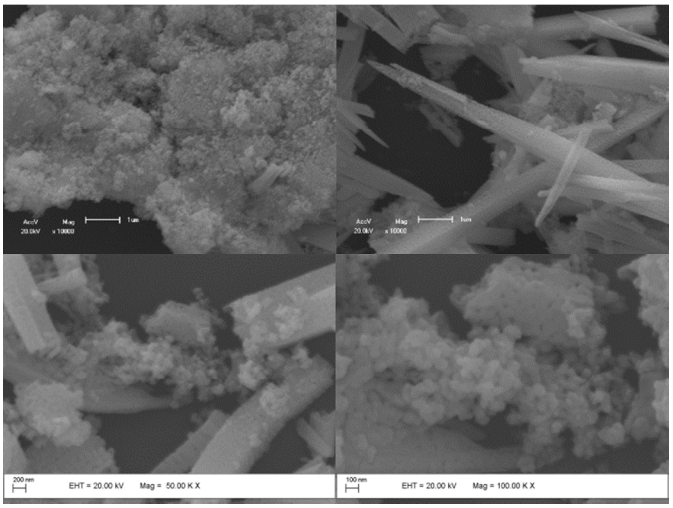

(A)

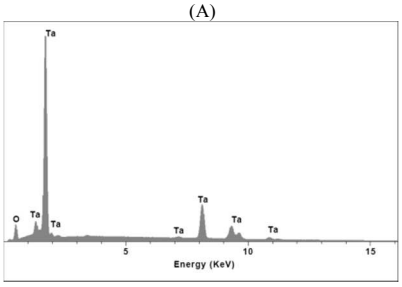

(B)

Figure 10. SEM micrographies (A) and EDS analysis (B) of the complexes TaTTA annealed at 900 °C for 4 h.

Conclusions

We successfully prepared a new series of tantalum(V)-β-diketonates complexes, using a simple and inexpensive method, based on aqueous $[TaF_7]^{2-}$ solution as tantalum precursor and TTA, HFA, or BFA. The complex originated in basic pH, achieved through addition of urea to the reactional medium and subsequent decomposition. The gradual in situ thermal decomposition of urea elicited not only the β–diketonate bond, but also the coordination of amino groups.

The optimized geometry of TaTTA and its calculated theoretical infrared spectrum served as a basis to determine its structure, which was $[TaTTA(NH_3)_3F_2]F_2$. The experimental results corroborated the optimized structure, especially the mass spectrometry, elemental analysis, and H^1-NMR data, which not only confirmed the presence of one TTA ligand and three NH_3 ligands, but also attested to the removal of the enolic proton TTA, and thus the coordination to tantalum. Conductivity measurements corroborated the presence of three ions in all the complexes, and the measured content of fluoride ions revealed the presence of two counterions. The structures of the complexes were solved as follows: $[TaTTA(NH_3)_3F_2]F_2$, $[TaHFA(NH_3)_3F_2]F_2$, and $[TaBFA(NH_3)_3F_2]F_2$.

The complexes exhibited blue emission at room temperature in both the solid state and in solution upon irradiated with UV light, a result of the heavy atom effect. The electronic properties of the complexes depended on the solvent, so these complexes constitute potential optical ethanol or humidity sensors. The absorption and emission spectra of the β-diketonates changed upon complexation with Ta. The bands related to the π-π* electronic transitions underwent bathochromic shift upon increasing solvent polarity, attributed to smaller energy difference between these two states due to stabilization of the excited state. This feature makes the complexes potentially applicable in the field of humidity/ethanol optical sensors.

The blue emission at room temperature in the solid state revealed promising application of the β-diketonate complexes in luminescent devices. Furthermore, TaBFA can serve as precursor to prepare nanostructured pure orthorhombic Ta_2O_5.

Acknowledgements

The authors thank *Companhia Industrial Fluminense-LTDA* for providing the tantalum fluoride compound and Prof. Norberto Peporini Lopes for the MALDI measurements. The authors would like to acknowledge FAPESP and CNPq for financial support. A.P. Ramos thanks Fapesp for her post-doctoral scholarship. The authors also acknowledge Mrs. Cynthia Maria de Campos Prado Manso and Dr. Rafael I. Estrada Mejia for reviewing the text and for helpful discussions.

Notes and references

[a] *Departamento de Química- Faculdade de Filosofia, Ciências e Letras de Ribeirão Preto- Universidade de São Paulo.*
DOI: 10.1039/b000000x/

1. S. I. Weissman, *Journal of Chemical Physics*, 1942, **10**, 214-217.
2. R. A. Vigato, V. Peruzzo and S. Tamburini, *Coordination Chemistry Reviews*, 2009, **253**, 1099-1201.
3. A. K. Narula, B. Singh, P. N. Kapoor and R. N. Kapoor, *Synthesis and Reactivity in Inorganic and Metal-Organic Chemistry*, 1983, **13**, 887-898.
4. H. O. Davies, T. J. Leedham, A. C. Jones, P. O'Brien, A. J. P. White and D. J. Williams, *Polyhedron*, 1999, **18**, 3165-3172.
5. L.-C. Liang, L.-C. Cheng, T.-L. Tsai, C.-H. Hu and W.-H. Guo, *Inorganic Chemistry*, 2009, **48**, 5697-5703.

6. M. Hayatifar, F. Marchetti, G. Pampaloni and S. Zacchini, *Inorganic Chemistry*, 2013, **52**, 4017-4025.
7. D. Bayot and M. Devillers, *Coordination Chemistry Reviews*, 2006, **250**, 2610-2626.
8. M. Kirihara, J. Yamamoto, T. Noguchi and Y. Hirai, *Tetrahedron Letters*, 2009, **50**, 1180-1183.
9. S. Nemana and B. C. Gates, *Catalysis Letters*, 2007, **113**, 73-81.
10. J. L. Ferrari, K. O. Lima, L. J. Q. Maia and R. R. Goncalves, *Thin Solid Films*, 2010, **519**, 1319-1324.
11. J. L. Ferrari, K. O. Lima, L. J. Q. Maia, S. J. L. Ribeiro, A. S. L. Gomes and R. R. Goncalves, *Journal of Nanoscience and Nanotechnology*, 2011, **11**, 2540-2544.
12. F. T. Aquino, R. R. Pereira, J. L. Ferrari, S. J. Lima Ribeiro, A. Ferrier, P. Goldner and R. R. Goncalves, *Materials Chemistry and Physics*, 2014, **147**, 751-760.
13. W. G. Quirino, C. Legnani, R. M. B. dos Santos, K. C. Teixeira, M. Cremona, M. A. Guedes and H. F. Brito, *Thin Solid Films*, 2008, **517**, 1096-1100.
14. A. Tsuboyama, H. Iwawaki, M. Furugori, T. Mukaide, J. Kamatani, S. Igawa, T. Moriyama, S. Miura, T. Takiguchi, S. Okada, M. Hoshino and K. Ueno, *Journal of the American Chemical Society*, 2003, **125**, 12971-12979.
15. C. Adachi, M. A. Baldo, M. E. Thompson and S. R. Forrest, *Journal of Applied Physics*, 2001, **90**, 5048-5051.
16. H. L. Wong, L. S. M. Lam, K. W. Cheng, K. Y. K. Man, W. K. Chan, C. Y. Kwong and A. B. Djurisic, *Applied Physics Letters*, 2004, **84**, 2557-2559.
17. W. S. Tang, X. X. Lu, K. M. C. Wong and V. W. W. Yam, *Journal of Materials Chemistry*, 2005, **15**, 2714-2720.
18. J. N. Demas and B. A. DeGraff, *Coordination Chemistry Reviews*, 2001, **211**, 317-351.
19. D. Wexler and J. I. Zink, *Inorganic Chemistry*, 1996, **35**, 4064-&.
20. A. Strasser and A. Vogler, *Inorganic Chemistry Communications*, 2004, **7**, 528-530.
21. H. Kunkely and A. Vogler, *Chemical Physics Letters*, 2000, **319**, 486-488.
22. S. N. Britvin, O. I. Siidra, A. Lotnyk, S. V. Krivovichev and W. Depmeier, *European Journal of Inorganic Chemistry*, 2010, 1082-1088.
23. C. C. Torardi, L. H. Brixner and G. Blasse, *Journal of Solid State Chemistry*, 1987, **67**, 21-25.
24. R. J. Candal, A. E. Regazzoni and M. A. Blesa, *Journal of Materials Chemistry*, 1992, **2**, 657-661.
25. A. Pedretti, L. Villa and G. Vistoli, *Journal of Computer-Aided Molecular Design*, 2004, **18**, 167-173.
26. A. Pedretti, L. Villa and G. Vistoli, *Journal of Molecular Graphics & Modelling*, 2002, **21**, 47-49.
27. A. Pedretti, L. Villa and G. Vistoli, *Theoretical Chemistry Accounts*, 2003, **109**, 229-232.
28. J. P. Perdew, K. Burke and M. Ernzerhof, *Physical Review Letters*, 1997, **78**, 1396-1396.
29. R. Ditchfie, W. J. Hehre and J. A. Pople, *Journal of Chemical Physics*, 1971, **54**, 724-&.
30. L. E. Roy, P. J. Hay and R. L. Martin, *Journal of Chemical Theory and Computation*, 2008, **4**, 1029-1031.
31. M. J. Frisch, G. W. Trucks, H. B. Schlegel, G. E. Scuseria, M. A. Robb, J. R. Cheeseman, J. A. Montgomery, T. V. Jr., K. N. Kudin, J. C. Burant, J. M. Millam, S. S. Iyengar, J. Tomasi, V. Barone, B. Mennucci, M. Cossi, G. Scalmani, N. Rega, G. A. Petersson, H. Nakatsuji, M. Hada, M. Ehara, K. Toyota, R. Fukuda, J. Hasegawa, M. Ishida, T. Nakajima, Y. Honda, O. Kitao, H. Nakai, M. Klene, X. Li, J. E. Knox, H. P. Hratchian, J. B. Cross, C. Adamo, J. Jaramillo, R. Gomperts, R. E. Stratmann, O. Yazyev, A. J. Austin, R. Cammi, C. Pomelli, J. W. Ochterski, P. Y. Ayala, K. Morokuma, G. A. Voth, P. Salvador, J. J. Dannenberg, V. G. Zakrzewski, S. Dapprich, A. D. Daniels, M. C. Strain, O. Farkas, D. K. Malick, A. D. Rabuck, K. Raghavachari, J. B. Foresman, J. V. Ortiz, Q. Cui, A. G. Baboul, S. Clifford, J. Cioslowski, B. B. Stefanov, G. Liu, A. Liashenko, P. Piskorz, I. Komaromi, R. L. Martin, D. J. Fox, T. Keith, M. A. Al-Laham, C. Y. Peng, A. Nanayakkara, M. Challacombe, P. M. W. Gill, B. Johnson, W. Chen, M. W. Wong, C. Gonzalez and J. A. Pople, *Gaussian 03, Revision B.04*, (2003) Gaussian Inc., Pittsburgh PA.
32. A. Werner, *Z. Phys. Chem. (Leipzig)*, 1893.
33. W. J. Geary, *Coordination Chemistry Reviews*, 1971, **7**, 81-&.
34. B. A. Uzoukwu, *Inorganica Chimica Acta*, 1990, **176**, 143-148.
35. W. F. Sager, Filipesc.N and F. A. Serafin, *Journal of Physical Chemistry*, 1965, **69**, 1092-&.
36. A. Strasser and A. Vogler, *Journal of Photochemistry and Photobiology a-Chemistry*, 2004, **165**, 115-118.
37. J. L. Ferrari, K. O. Lima, L. J. Q. Maia, S. J. L. Ribeiro and R. R. Goncalves, *Journal of the American Ceramic Society*, 2011, **94**, 1230-1237.
38. J. Liu, A. Wei, X. Zhao and H. Zhang, *Bulletin of Materials Science*, 2011, **34**, 443-446.
39. H.-C. Huang and T.-E. Hsieh, *Journal of Applied Polymer Science*, 2010, **117**, 1252-1259.